Magazine of Concrete Research

Failure assessment of flat slab-to-column members
Gosav, Kiss, Oneţ and Bompa

Magazine of Concrete Research
http://dx.doi.org/10.1680/jmacr.15.00405
Paper 1500405
Received 22/09/2015; revised 04/12/2015; accepted 05/12/2015
Keywords: failure/punching/slabs & plates

ice
Institution of Civil Engineers
publishing

Failure assessment of flat slab-to-column members

Andrei V. Gosav
Technical University of Cluj-Napoca, Romania
Zoltan I. Kiss
Technical University of Cluj-Napoca, Romania
Traian Oneţ
Technical University of Cluj-Napoca, Romania
Dan V. Bompa
Imperial College London, UK
(Corresponding author: d.bompa@imperial.ac.uk)

This paper is concerned with the ultimate behaviour of isolated flat slab members at the connection to interior columns. An experimental programme that focuses on the response of two-way members with various material and geometric configurations is presented. A full account of the results of ten scale tests comprising members with and without transverse reinforcement as double-headed shear studs is given. After describing the experimental arrangement and specimen details, the results and observations obtained from tests are provided and discussed. Particular attention is given to the influence of a number of key parameters that characterise the behaviour at the ultimate state such as slab thickness, layout and amount of the flexural and transverse reinforcement. The test results enable direct assessment of the governing factors that affect the behaviour and failure mode of flat slab members at the connection to interior columns. Finally, experimental results and observations are used to assess the adequacy of strength predictions obtained from analytical models currently adopted in design.

Notation

a	distance between slab edge and first yield line
A_{sw}	shear reinforcement contribution
b_c	column size
b_s	width of support strip
b_0	critical perimeter length
d	average effective bending depth $d = (d_x + d_y)/2$
d_{bw}	transverse bar diameter
d_{g0}	reference aggregate size
$d_{g,max}$	maximum aggregate size
d_v	shear effective depth
E_s	longitudinal reinforcement steel elastic modulus
E_{sw}	transverse reinforcement steel elastic modulus
f_{bd}	design bond strength
f_c	concrete compressive strength
f_{ct}	concrete tensile strength
f_u	ultimate longitudinal steel strength
f_{uw}	ultimate transverse steel strength
f_y	yield longitudinal steel strength
f_{yw}	yield transverse steel strength
h	slab thickness
h_{bw}	stud length
k_{dg}	size effect factor
k_e	eccentricity parameter
k_{sys}	coefficient accounting for performance of punching shear reinforcement system
k_ψ	rotational parameter
L	slab side size
l_s	isolated member moment span
l_0	critical crack length
m	moment
m_r	radial moment
m_R	plastic moment per unit length
m_S	average bending moment acting in support strip
m_φ	tangential moment
n_{bw}	number of transverse bars
n_{perim}	number of perimeters of transverse bars
r_c	column radius
r_D	radial surface strain in the diagonal direction
r_o	radial surface strain in the orthogonal direction
r_q	loading radius
r_s	slab radius
s_w	headed shear stud spacing
$s_{w,0}$	distance from column face to first perimeter of transverse bars
$s_{w,i}$	distance between headed shear studs outside of $S_{w,0}$
t_D	tangential surface strain in the diagonal direction
t_O	tangential surface strain in the orthogonal direction
V_c	punching shear strength for members without transverse bars, or the concrete contribution to punching shear strength for members with transverse bars
V_{flex}	flexural strength
V_R	punching shear strength
$V_{R,max}$	punching shear strength due to concrete crushing
V_s	contribution of transverse reinforcement to punching shear strength
V_{test}	test strength
w	crack width
x, y	orthogonal coordinates

α_s	function of the column location in the slab
β	ratio of long to short side of the column
β_w	transverse bar inclination
δ_{Vu}	slab deflection at the ultimate state
$\varepsilon_{y,sw}$	yield strain of transverse reinforcement
κ	critical shear crack opening factor
λ	factor
σ_{sw}	stress in the transverse reinforcement
ρ_l	average flexural reinforcement ratio $\rho_l = (\rho_{lx}\rho_{ly})^{1/2}$
ψ	slab rotation
χ	curvature

Introduction

The rapid development of the building industry resulted in the need for innovative, safe and optimised structural systems. Flat slabs, which have been used since the late nineteenth century, are one of the most popular systems used for structural applications. Their use is known to have the advantages of a short construction process and good functionality. From a structural point of view, flat slabs are governed by large deflections at the serviceability state and punching shear at the ultimate state. One of the common ways to overcome the brittle failure in the slab–column connection region is the addition of transverse bars. Common transverse reinforcement systems involve stirrups, inclined bars, hooks, steel profile cuts and headed shear studs. Owing to their good bond capacity and practicality compared with conventional stirrups, headed shear studs are one of the most attractive shear reinforcement systems available. In this study, members with double-headed shear studs welded to steel rails were investigated and analysed, and compared with members without shear reinforcement. A typical geometry and reinforcement arrangement of the tested specimens is shown in Figure 1.

The potential failure modes of a flat slab–column connection are flexural failure and punching shear failure. In the case of slabs without transverse reinforcement, the punching shear failure is characterised by low stresses in the longitudinal reinforcement and the development of a diagonal crack with variable inclination, starting from the root of the column to the tension face of the slab (Figure 2(a)). The inclination of the failure surface is dependent on the reinforcement ratio, slab thickness and material strength and characteristics (Bompa and Oneţ, 2015). When transverse reinforcement is present, the critical crack might intersect the transverse bars and result in yielding of the transverse reinforcement. This failure mode is known as 'punching within the shear-reinforced zone' (Figure 2(b)). In some cases, the critical crack passes below the transverse reinforcement and continues towards the tension face of the slab, away from the region with transverse bars. In this case, the punching shear failure occurs outside the shear-reinforced zone (Figure 2(c)). Punching shear failure can also be triggered by crushing of the compression strut that develops between the root of the column and the first perimeter of the transverse bars (Figure 2(d)). The flexural failure is governed by large deflections and yielding of the longitudinal reinforcement, for slabs both with and without transverse reinforcement (Figures 2(e) and 2(f)).

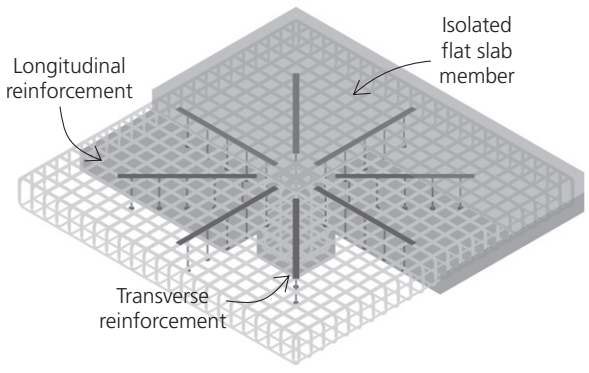

Figure 1. Isolated flat slab–column member

Previous investigations carried out on flat slabs without shear reinforcement have involved mainly thin slabs, which are rarely used in practice. Elstner and Hognestad (1956) reported a test series of 39 specimens in which the variables investigated were concrete strength, flexural reinforcement ratio, amount of compression reinforcement and column size. It was shown that the punching shear strength is primarily dependent on the concrete strength. Tests on circular flat slabs supported by circular columns and provided with ring or orthogonal longitudinal reinforcement were carried out by Kinnunen and Nylander (1960). They used their results as the basis for a mechanical model that is able to predict the deformational response, flexural strength and punching shear strength of such elements. Moe (1961) tested 43 typical slab configurations, of which some were provided with holes in the column vicinity to investigate the mechanism of failure. Later, the effect of slab size on the punching shear strength was investigated by Bazant and

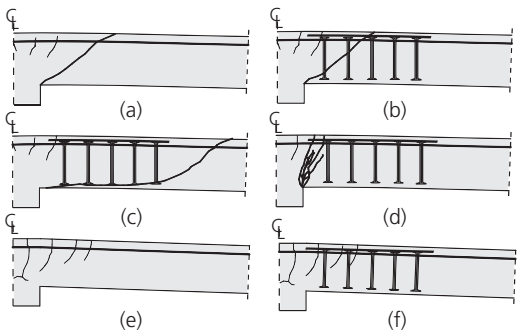

Figure 2. Potential failure modes: (a) punching shear for slabs without shear reinforcement; (b) punching shear within the shear-reinforced region; (c) punching outside the shear-reinforced region; (d) concrete crushing for slabs with shear reinforcement; (e) flexural failure; (f) flexural failure in the presence of shear reinforcement

Cao (1987). More recently, investigative work has been focused mainly on practical slab configurations. Tolf (1992) investigated a series of thick members, and showed that the nominal punching capacity decreases as member size increases. Hallgren (1996) undertook a numerical analysis of experimental results for members made of high-strength concrete and further used these in analytical models. Tests reported by Guandalini *et al*. (2009) investigated the behaviour of full-scale slabs with low amounts of flexural reinforcement.

Studies on members with transverse reinforcement have been carried out to investigate the effectiveness of various reinforcing systems and their contribution to the punching shear strength. The influence of slab thickness in the presence of orthogonally placed transverse studs was reported by Birkle and Digler (2008). Beutel and Hegger (2002) studied the effect of anchorage on the effectiveness of the shear reinforcement in the punching zone. A theoretical model for estimating the punching shear resistance of reinforced concrete flat slabs with shear reinforcement for concentric loading was proposed and validated in 12 full-scale specimens by Gomes and Regan (1999a, 1999b). They showed that the punching strength of slabs doubles if they are transversely reinforced with offcuts of rolled steel I-section beams. Carvalho *et al*. (2011) showed that both the strength and the ductility of post-tensioned flat slabs increases in the presence of stud rail reinforcement. Eligehausen *et al*. (2003) verified the behaviour of members provided with lattice girders as a transverse reinforcement system. Rizk *et al*. (2011) found that the addition of stud rail shear reinforcement to thick slabs modified the failure mode from punching shear to flexure. Lips *et al*. (2012) varied the thickness and amount of transverse reinforcement in 16 slab specimens to investigate the behaviour of the slab specimens, the activation of the shear reinforcement, and the strains developed in the shear-critical region at failure.

Although several investigators have analysed and compared sets of experimental results with existing analytical models, most studies have focused solely on ultimate strength, and recent ones have dealt with the member deformability and behaviour up to the ultimate state. Furthermore, few data have been reported in the literature regarding the activation of the transverse bars and their physical contribution to the punching shear strength. The experimental results obtained in the present study contribute to the existing test database, and the test observations advance the state-of-the-art regarding the behavioural aspects of flat slab members.

In this paper, a series of ten large-scale reinforced concrete flat slabs with various geometric and material configurations are presented. The purpose of the tests was to study the influence on slab behaviour of the slab thickness, flexural reinforcement ratio, and the amount and layout of the transverse reinforcement. The slabs showed failure modes varying from flexure to punching shear. After describing the specimens and the test rig characteristics, the experimental results and observations are analysed and discussed. Particular emphasis is given to the governing factors that affect the behaviour and failure mode of the slabs. In addition, the test results were used to assess the adequacy of strength predictions obtained from analytical models that are currently adopted in design. Limit analysis was used for the estimation of the flexural strength, and existing design or assessment guidelines were accounted for in the calculations of the punching shear strength (ACI 318-14 (ACI, 2014); Eurocode 2 (EC2) (CEN, 2004); Fernandez and Muttoni (2009); Model Code 2010 (fib, 2012); Muttoni (2008)).

Experimental programme

A series of ten tests on interior flat slab–column connections with and without shear reinforcement was carried out in two phases. The first test series consisted of five specimens (DB1–DB5) with the same slab thickness $h = 170$ mm and a low flexural reinforcement ratio. Four of the specimens were provided with transverse reinforcement: two specimens with double-headed shear studs welded on rails, and two with stirrup (or hook) beams placed between the flexural reinforcement layers. The fifth specimen had no transverse reinforcement. The second test series consisted of five specimens of varying thicknesses ($h = 200$–260 mm) and a high flexural reinforcement ratio. Three of the specimens in the second test series were provided with transverse reinforcement, while the other two had none.

The members tested replicate the connection region between interior columns and a continuous flat slab structure, with a moment span of about 4·5 m and a slab thickness commonly used in practice. The isolated member moment span represents the zero bending moment line, and was dictated by the test-rig limitations. The experimental programme is part of an ongoing research project at the Technical University of Cluj-Napoca investigating the ultimate behaviour of flat-slab specimens subjected to monotonic concentrated load.

Specimen details

As shown in Figure 3, the specimens had two in-plane configurations. The first test series consisted of five $1{\cdot}5 \times 1{\cdot}5$ m slabs of 170 mm thickness. The second series consisted of six $2{\cdot}2 \times 2{\cdot}2$ m specimens of variable thickness (200, 230 and 260 mm). At their centres, the slabs were connected to square column stubs with a cross-section of 300×300 mm. Both the top and bottom longitudinal reinforcement of specimens DB1, DB4 and DB5 consisted of 10 mm bars equally spaced at 100 m intervals, resulting in a flexural reinforcement ratio $\rho_l = 0{\cdot}54\%$. Specimens DB2 and DB3 had two supplementary 10 mm bars as connecting rods in the shear reinforcement system, the centroids of the bars being at 50 mm from the top face of the slab, resulting in a flexural reinforcement ratio $\rho_l = 0{\cdot}66\%$. The 200 mm thick specimens (AG1 and AG4) were

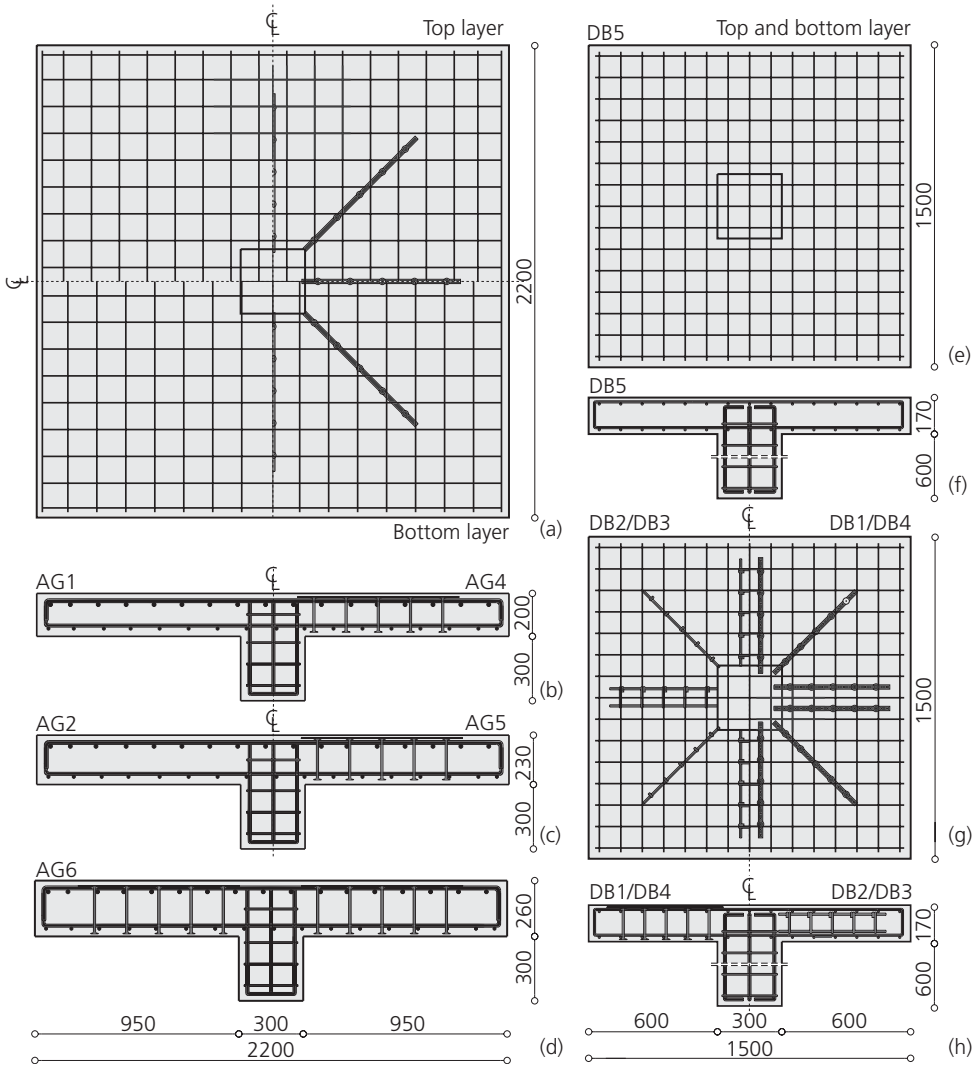

Figure 3. Geometry and layout of the longitudinal reinforcement of the test specimens

provided with eight 18 mm bars per unit metre on the top face, while specimens AG2 and AG5 had nine and specimen AG6 had eleven 18 mm bars per unit metre. In the case of specimens AG1–AG6, the reinforcement ratio was maintained constant at $\rho_l = 1{\cdot}24\%$ (Figure 3). All reinforcement bars were made of structural steel of S500 grade (Table 1). The bars were placed in an orthogonal arrangement. For the 170 mm specimens, the clear cover was 15 mm for both top and bottom reinforcement, whereas for the other specimens the cover for top reinforcement was 25 mm and that for the bottom reinforcement was 15 mm.

Specimens AG1, AG2 and DB5 had no transverse reinforcement (Figures 3(a)–3(e)). The other specimens were transversely reinforced with stud rail shear reinforcement (AG4–AG6 with the JDA-S Jordahl system, DB1 and DB4 with an in-house welded system) or stirrup beams encased between the longitudinal reinforcement layers (DB2 and DB3). The shear reinforcement was arranged in a star–like shape (Figures 3(a)–3(g)). The critical region was reinforced with five perimeters of bars having a diameter $d_{bw} = 10$ mm. The double-headed shear studs were made of S500 steel connected with a perforated strip made of structural steel, whereas the stirrup beams consisted of stirrups placed on four 10 mm longitudinal bars. In the case of 170 mm thick specimens, the spacing between the transverse bars was $s_w = 100$ mm, whereas for the thicker ones it was $s_w = 150$ mm (Table 2). The longitudinal reinforcement in the stub column consisted of eight 14 mm bars positioned at the corners and centres of the column, whereas the transverse reinforcement was composed of 10 mm stirrups evenly spaced at $s_w = 100$ mm.

The first set of specimens (DB) were prepared and cast in place in three batches using normal concrete C20/25 with a

Specimen	h: mm	d: mm	$b_{c1} = b_{c2}$: mm	ρ_l: %	f_c: MPa	f_{ct}: MPa	f_y/f_u: MPa	V_{test}	V_{test}/V_{flex}	FM[a]
DB1	170	145	300	0·54	25·1	1·71	521/636	517	1·07	F
DB2	170	145	300	0·66	34·9	1·99	521/636	557	0·94	F
DB3	170	145	300	0·66	18·2	1·49	521/636	561	1·00	F
DB4	170	145	300	0·54	24·4	1·58	521/636	527	1·09	F
DB5	170	145	300	0·54	35·1	2·12	521/636	495	1·01	FP
AG1	200	157	300	1·25	17·5	1·27	583/685	570	0·51	P
AG2	230	187	300	1·24	19·2	1·48	583/685	872	0·54	P
AG4	200	157	300	1·25	21·6	1·86	583/685	727	0·62	P
AG5	230	187	300	1·24	23·8	2·18	583/685	1008	0·60	P
AG6	260	217	300	1·24	22·6	2·01	583/685	1328	0·59	P

[a]FM, assumed failure mode; F, flexure; FP, flexural punching; P, punching

Table 1. Specimen details and ultimate strengths

Specimen	Reinforcement system	d_{bw}: mm	$n_{bw/perim}$	n_{perim}	$s_{w,0}$: mm	$s_{w,i}$: mm	h_{bw}: mm	f_{yw}/f_{uw}: MPa
DB1	DHSR	10	12	5	40	100	150	355/–
DB2	ST-B	10	12	5	40	100	100	355/–
DB3	ST-B	10	12	5	40	100	100	355/–
DB4	DHSR	10	12	5	40	100	150	355/–
AG4	DHSR	10	8	5	50	150	155	525/623
AG5	DHSR	10	8	5	60	150	185	525/623
AG6	DHSR	10	8	5	70	150	215	525/623

Table 2. Details of shear reinforcement systems

maximum aggregate size of 16 mm; ready mixed concrete was used for the second set of specimens (AG). Average concrete compressive and tensile strength determined from material tests are given in Table 1. The compression and splitting material tests were carried out on a minimum of three samples at 28 days and on the day of the test on cubes with sides of 150 mm. Additional material tests on prismatic specimens were carried out to assess the tensile strength by means of flexural tests. The cylinder compressive strength was calculated using a correspondence factor between cylinder and cube strength of 0·8, and the concrete elastic modulus was computed according to Model Code 2010 provisions (fib, 2012). Tension tests on steel bar coupons were carried out to assess the yield and ultimate strength of the longitudinal and transverse reinforcement (Tables 1 and 2). The elastic modulus of the reinforcement steel was assumed to be $E_s = E_{sw} = 200$ GPa.

Test set-up

The test rig comprised a stiff tri-dimensional frame that acted as support for the specimen, and a reaction frame to hold the actuator (Figure 4). The dimension of the supporting frame varied with the in-plane dimensions of the specimens. All the

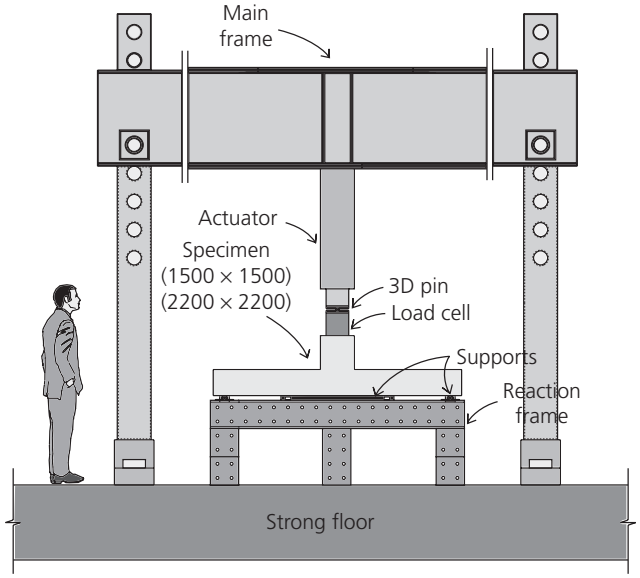

Figure 4. Schematic representation of the test setup

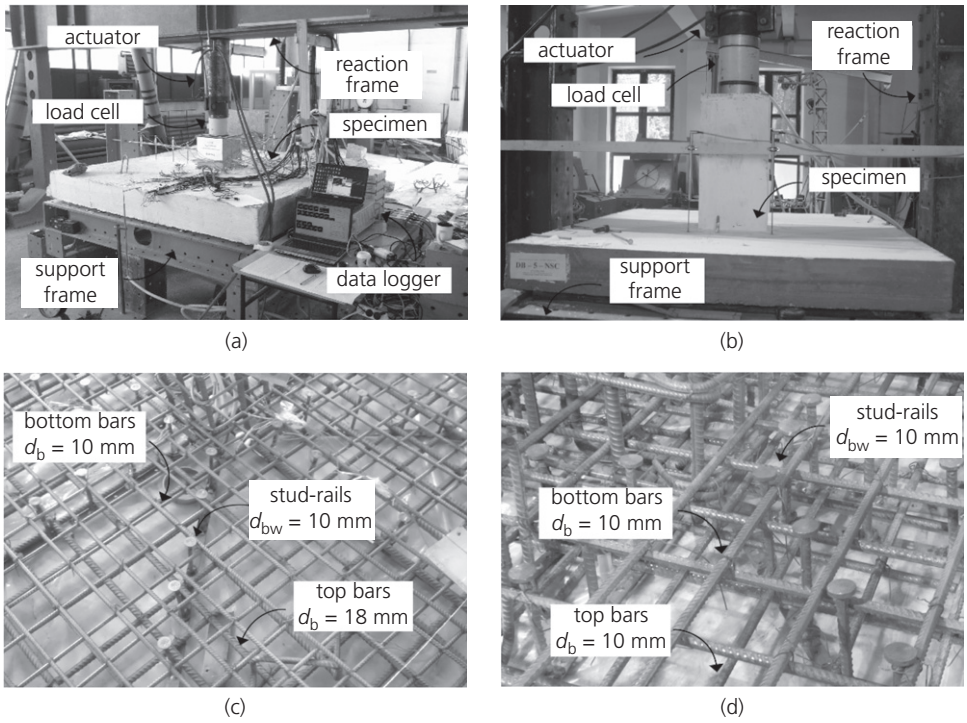

Figure 5. Test rig and instrumentation for: (a) test series 2 (AG); (b) test series 1 (DB). Reinforcement layout: (c) test series 2 (AG); (d) test series 1 (DB)

specimens were tested upside down with the load introduced over the column, simulating the case without moment transfer to the slab. The slabs were simply supported on linear supports, resulting in a member moment span of 1450 mm for the first test series (DB1–DB5) and 2000 mm for the second test series (AG1–AG6). The load was applied directly to the column by means of a hydraulic actuator and was instrumented with a load cell with a capacity of 5 MN. The load was applied in increments of 10–25 kN depending on the predicted failure load. A series of electrical resistance strain gauges were used to measure strains on reinforcement and concrete as follows: four were placed on the longitudinal reinforcement, ten on the headed shear studs and four on the surface of the concrete (Figure 5). Mechanical gauge devices were attached to the top and bottom faces of the reinforced concrete slab to assess the surface strains. Thirteen inductive standard displacement transducers were used to assess the deflection and deflected shape following both orthogonal directions of AG specimens. For the DB specimens the deflection was recorded by means of three transducers. Crack patterns and crack widths were recorded in all tests up to a maximum crack width $w_{max} = 0{\cdot}4$ mm.

Experimental results and observations

Figures 6(a) and 6(b) show plots of the load versus the deflection response recorded during testing. The applied load represents the value recorded by the load cell. The displacement was recorded on the top face by the displacement transducer located at the centre of the specimen. The deflection response showed uniform behaviour throughout the entire loading process for all tested specimens. The stiffness of each specimen was influenced by slab thickness h and flexural reinforcement ratio ρ_l. The specimens with the low reinforcement ratio $\rho_l = 0{\cdot}5\%$ (DB1–DB5) showed the most flexible behaviour (Figure 6(a)), whereas those with the high reinforcement ratio $\rho_l = 1{\cdot}25\%$ developed stiffer behaviour, the stiffness increasing nearly proportionally with the thickness (Figure 6(b)). Flexural cracking was first observed at load levels of about 15–20% of the ultimate strength V_{test} in the case of specimens DB1–DB5. Specimens AG1 and AG2 exhibited flexural cracking at about 9–17% of V_{test}, whereas for AG4–AG6 this was observed at 19–23% of the specimens' ultimate strength. AG3 is not reported in this paper as some of the recorded test data were unreliable.

The deflection at failure, recorded by means of displacement transducers, was similar for each specimen type in the DB series (Figure 6(a)). The specimen without shear reinforcement (DB5) showed similar stiffness and deflection to the specimens provided with stud rail reinforcement (DB1 and DB4). Failure occurred at an applied load of $V_{test} = 495$ kN. A conical body dislocated from the specimen and remained suspended in the bending reinforcement. The failure was attributed to flexural punching.

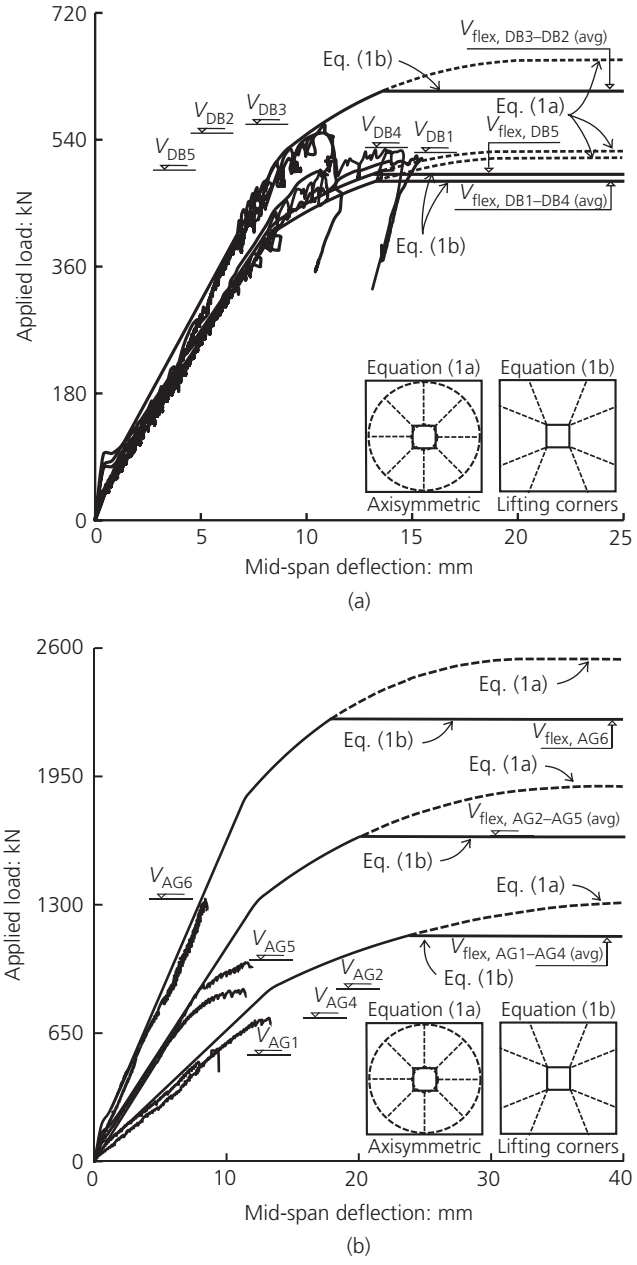

Figure 6. Load versus deflection at mid-span for the tested specimens and the predicted flexural response

Members DB1 and DB4 showed larger deflections but lower stiffness and ultimate strength, whereas DB2 and DB3 showed smaller deflections, higher stiffness and higher ultimate strength (Table 1). The enhanced performance of DB2 and DB3 resulted primarily from the presence of the supplementary reinforcement, used as connectors for the stirrups, which increased the flexural reinforcement ratio. The transversely reinforced specimens (DB1–DB4) failed at applied loads V_{test} of 517–561 kN.

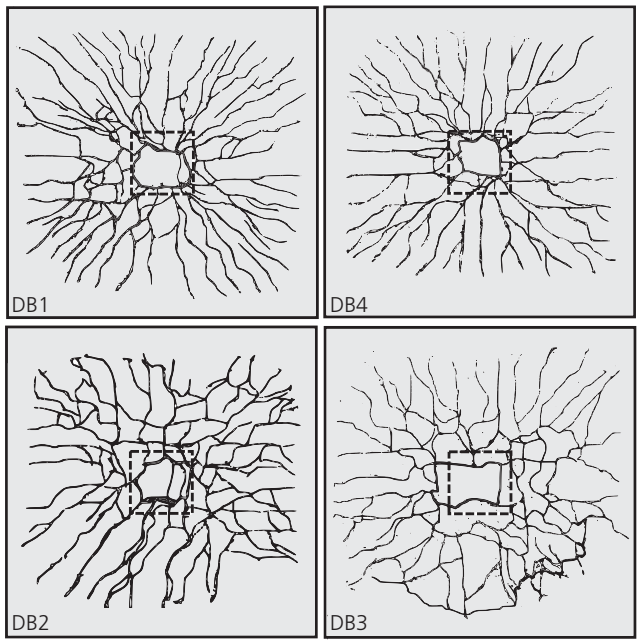

Figure 7. Crack patterns for specimens DB1–DB4, which had a low reinforcement ratio (test series 1)

The closed shape-governing cracks at the top face of the slab, located near the column region, are depicted in Figure 7 (the corresponding column edges at the bottom face are represented by dashed lines; the crack pattern is represented by continuous lines). Considering that the inclination of the critical crack is given by a surface that joins the root of the column to its pattern at the top, specimens DB1–DB4 showed crack angles at failure of about 90°. In addition, there were no records to show that the critical crack intersected any of the transverse bars. This suggests that flexural failure was the governing failure mode (fib, 2001).

The deflection behaviour of specimens AG1–AG6 can be grouped according to their thickness. The thinnest specimen ($h = 200$ mm) showed the most flexible behaviour, whereas the thickest one showed the stiffest behaviour ($h = 260$ mm). The ultimate strengths varied with the thickness and depended on the presence of the transverse reinforcement. For all specimens the failure was characterised by brittle behaviour and was attributed to punching shear. The recorded crack patterns at the ultimate state are depicted in Figure 8. Specimen AG1 showed the lowest ultimate strength in the AG series, with $V_{test} = 570$ kN and a corresponding deflection of $\delta_{Vu} = 9{\cdot}33$ mm. The analogous specimen with shear reinforcement (AG4) showed a 27% increase in strength $V_{test} = 727$ kN and a deflection at failure of 13·2 mm. An increase in stiffness was observed for specimens AG2 and AG4, which had ultimate strengths of 872 and 1008 kN, respectively. The mid-span deflection at failure was 11·3 mm for AG2 and 11·4 for AG5. Although transverse reinforcement was present in AG5, the

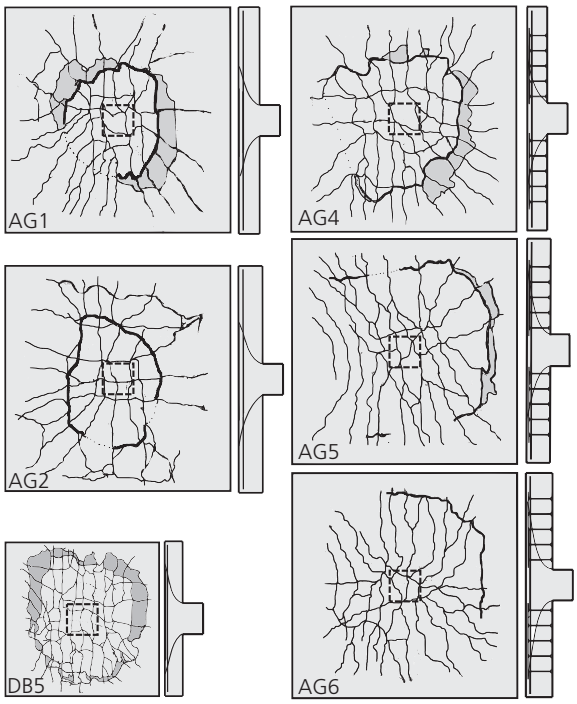

Figure 8. Crack patterns on the top surface and assumed crack patterns in section for the AG specimens

ultimate strength and deflection response were similar to those for AG2. The highest strength was seen for specimen AG6 (1328 kN). However, the deflection at failure for this specimen had the lowest value of all the AG specimens (8·37 mm). As a result of slab geometry and load arrangement, at the ultimate state specimens AG5 and AG6 showed a slight non-symmetric behaviour.

For AG specimens, the strains in the transverse reinforcement, recorded by means of electrical strain gauges, showed values above yield strain in at least one of the studs, whereas the strain in the longitudinal bars remained within elastic limits (Figures 9(a)–9(c)). The failure is attributed to punching within the shear-reinforced area. According to the information obtained from the strain gauges, it appears that the failure was triggered by the activation of an instrumented headed shear stud located in the second perimeter (represented by black lines in Figures 9(a)–9(c)) at 87·1%, 90·6% and 55·7% of the ultimate applied load for AG4, AG5 and AG6, respectively. The strain diagrams in Figure 9(c) show that shear cracking initiated around 800 kN. Further propagation and growth of the critical crack resulted in the yield of bars located in the first or second perimeter.

The concrete tangential surface strains, recorded by means of mechanical devices (following orthogonal t_o and diagonal t_D directions) showed values above the corresponding design crushing strain ε_{c1} accounting for the concrete strength on the day of the test. On the other hand, the concrete radial surface strains, recorded by means of electrical strain gauges (following orthogonal r_o and diagonal r_D directions) showed values up to a quarter of the crushing strain ε_{c1} (Figures 9(d) and 9(e) – specimens AG1 and AG4).

Ultimate behaviour and strength

This section deals with the assessment of the deformational behaviour and ultimate strength of the members described in the preceding sections. The load–rotation response was assessed using the analytical model developed by Muttoni (2008). The flexural strength was assessed by considering the minimum of the predictions of two yield line mechanisms, and was compared further with the test strength. A ratio of the test strength to flexural strength V_{test}/V_{flex} higher than unity indicates bending-controlled failures, while values below unity indicate failure due to punching shear. Regardless of the mode of failure, when comparing the predicted and experimental load–rotation diagrams it was considered that constant rotations developed within the assumed slab radius. In cases when the ultimate test rotation was smaller than the predicted yield rotation, an assessment of punching shear strength was made, for members with and without transverse studs.

Load–rotation response and flexural strength

The flexural strength of a slab subjected to a load over a defined area (column) can be computed by means of upper bound limit analysis, which accounts for licit bending mechanisms. This is the case for the axisymmetric mechanisms that can be used to obtain the load–rotation response and flexural strength of a slab (Kinnunen and Nylander, 1960; Muttoni, 2008). The methods account for a set of equilibrium equations between the applied load and the energy dissipated due to the rotation of the rigid sectors along the tangential and radial directions. The load–rotation is calculated by numerical integration of the moment–curvature (m–χ) relationship, assuming that the tangential cracks and the radial curvature are concentrated in the vicinity of the column.

The radial moment m_r is considered to be constant over a region with a radius r_0, whereas the tangential moment m_φ varies with the crack extension and yield. The m–χ relationships are independent and equal in the radial and tangential directions, and are assumed to be linear over four regions (quadrilinear) (Muttoni, 2008). The deflections can be obtained through accounting for a further integration step. The transfer of residual stresses between cracked interfaces is accounted for by adding the influence of tension stiffening to the cracked stiffness. The relationship between the orthogonal and axisymmetric layouts of the bending reinforcement is accounted for by a factor of 0·6. At the ultimate state, the flexural strength of the member is reached when the plastic moment, in both the tangential and the radial direction, is attained (Equation 1a) (Kinnunen and Nylander, 1960).

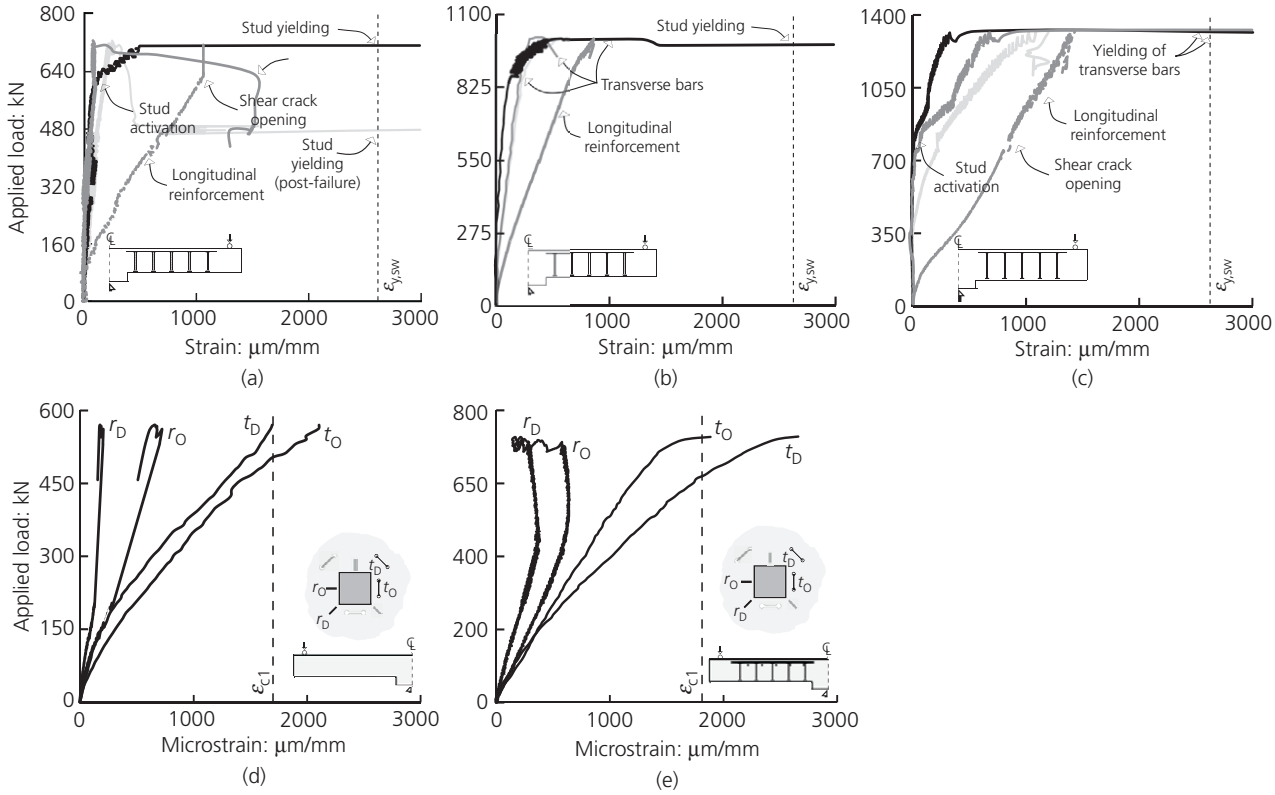

Figure 9. Strain values in the transverse and longitudinal reinforcement: (a) AG4; (b) AG5; (c) AG6. Tangential and radial strain: (d) AG1; (e) AG4

The analytical model requires the definition of the slab radius representing the zero-moment iso-line. The configuration of the supports allowed rotations in both orthogonal directions. In the case of square columns, the reaction force concentrates at the mid-span of the member, simulating a two-way behaviour with the corners of the slab free to lift. The length of the contact line between the support and the slab reduces with increasing load. An elastic analysis of the shear flow within specimen DB5, taking into account various contact lengths of the supports, from $b_c/2$ to l_s, showed a concentration of shear at the mid-span following both moment actions. Hence, it was assumed that the radius of the slab accounted for in the bending calculations was inscribed in the square shape formed by the supports. The slab radius of specimens DB1–DB5 was $r_q = 725$ mm, and that for members AG1–AG6 was $r_q = 1000$ mm.

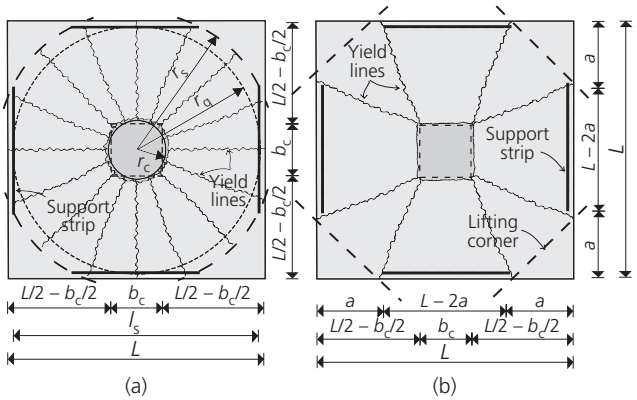

Figure 10. Yield line mechanisms: (a) axisymmetric; (b) lifting corners

The flexural strength of the test specimens was assessed using the yield line method, taking the minimum V_{flex} of the values obtained using the two yield line mechanisms depicted in Figure 10. In the case of the axisymmetric mechanism, the column radius r_c is $2b_c/\pi$, the slab radius r_s is $1{\cdot}074L/2$ and loading radius r_q is 725 and 1000 mm for specimens DB and AG, respectively (Figure 10(a)). The 'lifting corner' mechanism, depicted in Figure 10(b), is represented by Equation 1b (Elstner and Hognestad, 1956). The value of a, which represents the distance between the slab edge and the first yield line, was chosen to obtain the lower bound of the flexural strength. A numerical study showed that the minimum

is obtained for $a/L = 0{\cdot}23$ for DB specimens and $a/L = 0{\cdot}25$ for AG specimens.

1a. $$V_{\text{flex},1} = 2\pi m_{\text{R}} \frac{r_{\text{s}}}{r_{\text{q}} - r_{\text{c}}}$$

1b. $$V_{\text{flex},2} = 8m_{\text{R}} \left(\frac{L - 2a}{L - b_{\text{c}}} + \frac{a}{L - b_{\text{c}} - a} \right)$$

1c. $$V_{\text{flex}} = \min\left(V_{\text{flex},1}, V_{\text{flex},2}\right)$$

The load–mid-span deflection relationships for the DB specimens and the analytical prediction based on the axisymmetric model are plotted in Figure 6. The load–deflection response is plotted as the average value considering the type and layout of the longitudinal reinforcement of the specimens. At the ultimate state, according to the predictions of the axisymmetric mechanism (Equation 1a), the flexural strength of specimens DB1–DB5 varies between 515 and 670 kN, whereas according to the predictions of the 'lifting corner' mechanism (Equation 1b) it varies between 482 and 590 kN. Considering the minimum, the failure loads of specimens DB1–DB5 correspond to 89–109% of their flexural strength V_{flex} (Table 1). The deformation behaviour computed with the axisymmetric model is in good agreement with the recorded behaviour for all tests. For the reported specimens, at the ultimate state, the 'lifting corners' mechanism offers the lowest bound of the flexural strength.

These results, in conjunction with the crack patterns shown in Figure 7, suggest that flexural failure was the governing failure mode for specimens DB1–DB4 and that the contribution of transverse reinforcement to the ultimate strength was minimal. Even if the predicted flexural strength of specimen DB5 is similar to the recorded test strength, failure eventually occurred due to the dislocation of a punching cone, and was thus characterised as 'flexural punching' (Figure 8). Specimens AG1–AG6 reached their ultimate strengths at 36–62% of their flexural strengths, which indicates that failure was governed by punching shear.

Punching shear strength

This section deals with the assessment of the punching shear strength of flat slab members without and with shear reinforcement in the form of headed shear studs. The experimental findings of the present study enabled direct strength predictions of the members. The predictions obtained using the expressions available in EC2 (CEN, 2004), ACI 318-14 (ACI, 2014) and Model Code 2010 (fib, 2012) were analysed and compared with those obtained using the critical shear crack theory (CSCT) (Fernandez and Muttoni, 2009; Muttoni, 2008).

According to EC2 (CEN, 2004) provisions, the punching shear strength of reinforced concrete solid slabs without shear reinforcement and without prestressing (or other longitudinal force) is dependent on the concrete strength f_{c}, flexural reinforcement ratio ρ_{l} and the size effect $k = 1 + (200/d)^{1/2} \leq 2$ (Equation 2). The shear resistance is checked at the face of the column and at the basic control perimeter b_0 with rounded corners situated at $2d$ from the column face, where d is the effective bending depth.

The ACI 318-14 design code considers that the shear stress acting in the column vicinity is a function of the concrete strength f_{c}. It assumes a pseudo-critical section located at a distance $d/2$ from the column periphery. For non-prestressed slabs without shear reinforcement, such as those examined in the present study, the punching shear strength is the smallest of the three conditions in Equation 3, where β is the ratio of long side to short side of the column and α_{s} is a function of the column location in the slab ($\alpha_{\text{s}} = 40$ for interior columns).

2. $$V_{\text{c}} = 0{\cdot}18\left(1 + \sqrt{200/d}\right)(100\rho_{\text{l}} f_{\text{c}})^{1/3} b_0 d$$

3. $$V_{\text{c}} = \min[0{\cdot}17(1 + 2/\beta), 0{\cdot}083(\alpha_{\text{s}} d/b_0 + 2), 0{\cdot}33] b_0 d \sqrt{f_{\text{c}}}$$

The theory of Model Code 2010 is based on multiple levels of refinement depending on the required level of accuracy. For a general case, the shear-resisting control perimeter can be obtained on the basis of the shear fields. In typical situations such as the specimens investigated here, the basic control perimeter b_0 may be taken to be at a distance $0{\cdot}5d_{\text{v}}$ from the column sides (where d_{v} is the shear effective depth of the slab that accounts for the effective level of the support region). In Model Code 2010, the punching shear strength is a function of the parameter k_{ψ}, which depends on the slab rotation ψ and the size effect factor $k_{\text{dg}} = 32/(16 + d_{\text{g,max}}) > 0{\cdot}757$, where $d_{\text{g,max}}$ is the maximum aggregate size.

Other parameters required for the assessment of punching shear strength are: the distance between the zero bending moment line and the load application point r_{s}, calculated using a linear elastic model for level 3 of approximation (LoA3) (used here), the effective bending depth d, the design yield strength of bending reinforcement f_{y}, the steel modulus of elasticity E_{s}, the average bending moment acting in the support strip m_{S} (taken as the average value of the moment for design of the flexural reinforcement over the width of the support

strip b_s) and the plastic moment per unit length in the support strip m_R (Equation 4).

In the CSCT the punching shear strength of flat slabs without shear reinforcement is estimated by considering the intersection between the rotational response of the slab $V-\psi$ (here computed by means of the axisymmetric model Muttoni, (2008)) and the failure criterion provided by the method k_ψ (Equation 5). Similarly to Model Code 2010, it is considered that the critical section is located at $0{\cdot}5d_v$.

4a. $$V_c = k_\psi \sqrt{f_c} b_0 d_v$$

4b. $$k_\psi = 1/\left(1{\cdot}5 + 0{\cdot}9\psi d k_{dg}\right) \leq 0{\cdot}6$$

4c. $$\psi = 1{\cdot}2\frac{r_{s,i}}{d}\frac{f_y}{E_s}\left(\frac{m_{S,i}}{m_{R,i}}\right)^{3/2}$$

5. $$k_\psi = 0{\cdot}75/\left[1 + 15\psi d/\left(d_{g,max} + d_{g0}\right)\right]$$

At the ultimate state, members provided with shear reinforcement are prone to three potential punching shear failures: within the shear-reinforced region, outside the shear-reinforced region and by reaching the maximum punching capacity through strut crushing. Codified provisions consider that the governing punching shear strength is given by the minimum of these three (Equation 6a). For failures within the shear-reinforced region, the punching shear strength is assessed considering the cumulative contributions of concrete and of transverse reinforcement (Equation 6b). In some cases, codified provisions reduce the concrete contribution by a certain amount. For reasons of uniformity, this reduction is represented by factor λ ($0{\cdot}75$ for EC2, $0{\cdot}50$ for ACI 318-14). Model Code 2010 and the CSCT account for the contribution of concrete in full ($\lambda = 1{\cdot}00$).

6a. $$V_R = \min(V_{R,in}, V_{R,out}, V_{R,max})$$

6b. $$V_{R,in} = \lambda V_c + V_s$$

In Eurocode 2 the contribution of shear reinforcement A_{sw} is considered by accounting for one row of transverse bars located in the column vicinity and the reduced yield strength $f_{yw} = 250 + 0{\cdot}25d$ (Equation 7). ACI 318-14 accounts for the cumulative contribution of concrete and shear reinforcement that intersects a potential punching plane at $d/2$. The yield strength of the shear reinforcement is limited to $f_{yw} = 420$ MPa (Equation 8). Model Code 2010 accounts for a rotationally dependent contribution of the transverse reinforcement to the punching shear strength (Equation 9) (here the eccentricity parameter $k_e = 1{\cdot}0$ for concentric punching). The method assesses the stress in the transverse reinforcement, taking into consideration the slab rotation ψ, design bond strength f_{bd} (here 5 MPa), transverse bar diameter d_{bw} and yield strength f_{yw}, steel elastic modulus E_s and effective bending depth d.

In the CSCT, the contribution of the transverse reinforcement is calculated by considering that the opening of the shear critical crack is proportional to the product of the rotation of the slab ψ times the effective depth of the member, where $\kappa = 0{\cdot}5$ (Equation 10). The stress in the transverse reinforcement is a function of the crack opening w, the reinforcement geometry and type, and the bond conditions between the concrete and the rebar. The behaviour of double-headed shear studs in this investigation is characterised by three regimes depending on the crack width and the position of the stud relative to the tip of the crack (Fernandez and Muttoni, 2009).

7. $$V_s = 1{\cdot}5(d/s_w)A_{sw}f_{yw}\sin(\beta_w)$$

8. $$V_s = A_{sw}f_{yw}(d/s_w)$$

9a. $$V_s = \Sigma A_{sw}\sigma_{sw}k_e$$

9b. $$\sigma_{sw} = \frac{E_s\psi}{6}\left(1 + \frac{f_{bd}}{f_{yw}}\frac{d}{d_{bw}}\right) \leq f_{yw}$$

10a. $$w = \kappa\psi d$$

10b. $$V_s = \Sigma A_{sw}\sigma_{sw}(w, f_{bd})$$

Codified provisions represent the punching shear strength due to concrete crushing $V_{R,max}$ as a function of the concrete contribution V_c. ACI 318-14 accounts for a crushing strength as

two times the strength of a slab without shear reinforcement. In the case of EC2, the maximum punching strength is dependent on the concrete strength, effective bending depth, control perimeter and a factor that accounts for the governing strut capacity derived from the beam behaviour. For Model Code 2010 and the CSCT, the maximum punching shear resistance, which is limited by strut crushing, is a function of the concrete contribution V_c times a coefficient k_{sys} that accounts for the performance of the punching shear reinforcement system ($k_{sys} = 2{\cdot}0$ in the absence of experimental data).

Punching outside of the shear-reinforced zone $V_{R,out}$ occurs when the failure develops outside of the foremost perimeter of the transverse reinforcement. The verification varies with the code provision, and is made by taking into account an enlarged control perimeter situated at a distance from the border of the shear-reinforced region ($d/2$ for ACI, Model Code 2010 and the CSCT, $1{\cdot}5d$ for EC2).

Table 3 summarises the punching shear strength of the test specimens for the two failure modes observed during tests: punching without shear reinforcement (Equations 2–5) for specimens AG1, AG2 and DB5; and punching within the shear-reinforced region (Equation 6b) for specimens AG4–AG6. Overall, the current design provisions provide reliable strength predictions. In the case of specimens without transverse reinforcement, the deformation behaviour is captured faithfully by the CSCT and the strength is estimated well by the current design codes (Figures 11(a)–11(c)). For the specimens in the present study it was found that the ACI 318-14 design code gives conservative estimates, whereas EC2, Model Code 2010–LoA3 and the CSCT give similar results. The highest efficiency for members without transverse reinforcement seems to be obtained from the predictions of Model Code 2010–LoA3, with an average of 1·07 and a coefficient of variance of 8% compared with the experimental results presented earlier in this paper.

The predicted results for specimens with transverse reinforcement show good agreement with the test results, as the limits imposed on the yield strength of the transverse reinforcement are accounted for in EC2 and ACI 318-14. Also, the reduction in the concrete contribution in the case of shear-reinforced specimens (25% with EC2, 50% with ACI 318-14) plays an important role in the assessment procedure. For the tested specimens, EC2 gave an average of 1·13 and a scatter between results of 7%, whereas ACI 318-14 gave more conservative predictions. Model Code 2010–LoA3 and the CSCT gave nearly identical results, as Model Code 2010–LoA3 is the refined codified approach of the CSCT. LoA3 of Model Code 2010 offers reliable and accurate results as the calculation involves physical parameters and real material properties.

A previous study on an extended test database of isolated slab specimens without transverse reinforcement indicated that the punching shear strength decreases with decreasing concrete strength and effective bending depth/isolated member moment span (d/l_s) ratio, and increases with the flexural reinforcement ratio (Bompa and Oneţ, 2015) (the moment span of an isolated slab specimen is the distance between the supports, and is a function of the load arrangement and test setup). In a similar manner, all the tests reported in this paper, regardless of the failure mode, were compared as a function of the varied structural parameters. In Figure 12 the investigated parameters are plotted against the recorded test strength V_{test} in relation to member effective depth d, concrete strength f_c and critical crack length l_0, which is dependent on the inclination of the punching shear crack (Bompa and Oneţ, 2015). The data for members that failed in punching shear are plotted as dots

Type	Specimen	Test	EC2		ACI 318-14		Model Code 2010–LoA3		CSCT	V_{test}/V_R
		V_{test}	V_R	V_{test}/V_R	V_R	V_{test}/V_R	V_R	V_{test}/V_R	V_R	
Without transverse reinforcement	DB5	495	421	1·18	504	0·98	498	0·99	485	1·02
	AG1	570	500	1·14	395	1·44	542	1·05	521	1·09
	AG2	872	687	1·27	526	1·66	744	1·17	706	1·24
With transverse reinforcement	AG4	727	687	1·06	495	1·47	734	0·99	751	0·97
	AG5	1008	900	1·12	621	1·62	884	1·14	882	1·14
	AG6	1328	1097	1·21	733	1·81	1006	1·32	1020	1·30
	Average			**1·16**		**1·50**		**1·11**		**1·13**
	COV			**0·06**		**0·19**		**0·11**		**0·11**

Table 3. Assessment and comparison of the punching shear strengths

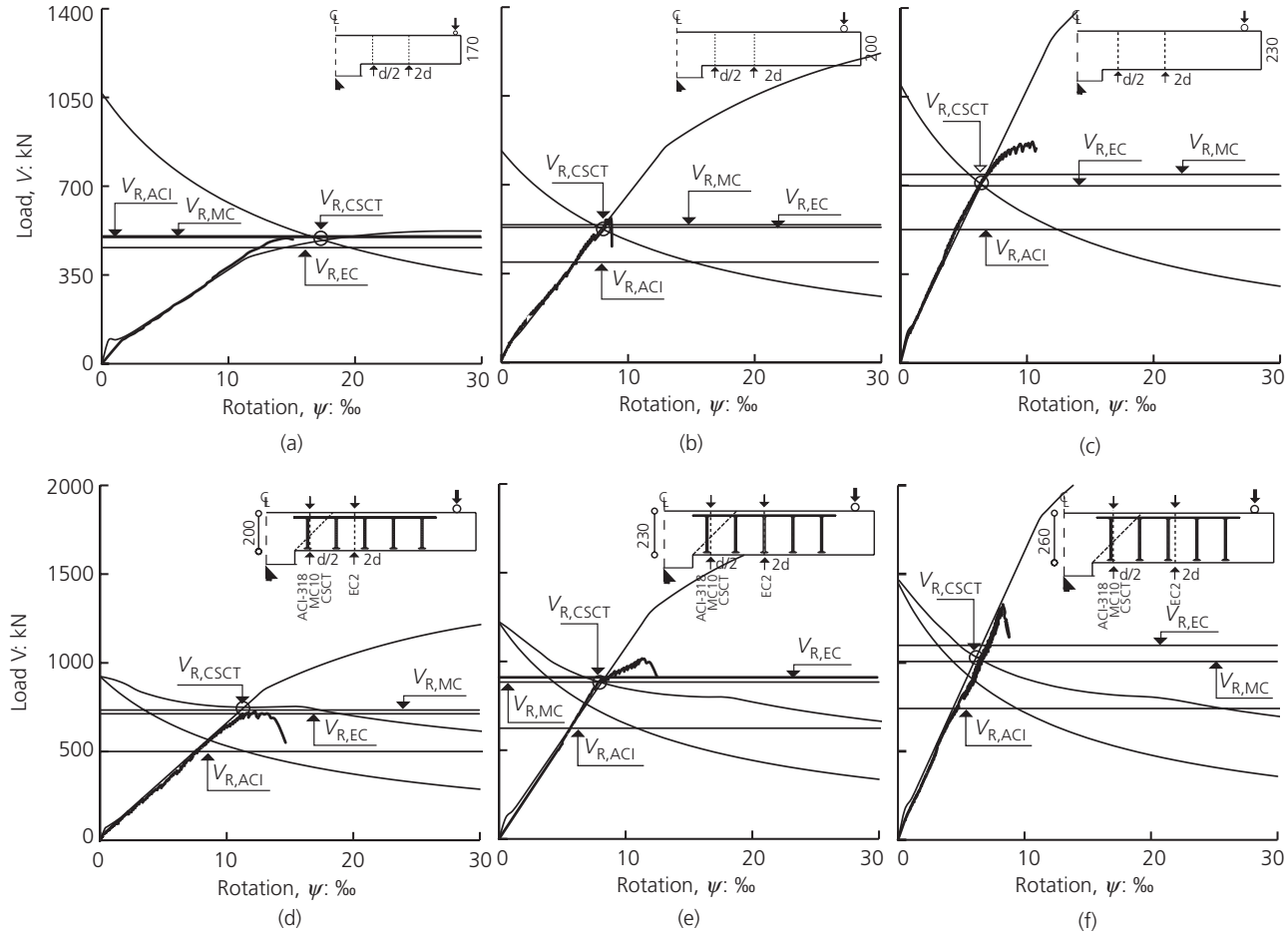

Figure 11. Punching shear strength predictions for the specimens: (a) DB5; (b) AG1; (c) AG2; (d) AG4; (e) AG5; (f) AG6

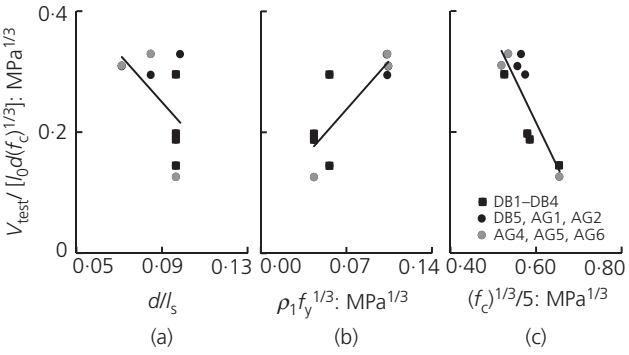

Figure 12. The influence of structural parameters on member response: (a) effective depth to isolated member moment span; (b) flexural reinforcement and yield strength; (c) concrete strength

(black for non-shear-reinforced specimens and grey for specimens with transverse bars) and black squares indicate specimens that failed in flexure.

It can be seen that flexible members with reduced slab thickness in relation to their isolated member moment span attained lower strengths and were generally governed by bending (Figure 12(a)). Low flexural reinforcement ratios, in conjunction with small thicknesses, could lead to flexural failure (Figure 12(b)). On the other hand, thick members with a high flexural reinforcement ratio failed in punching shear, even if they were shear reinforced. The increase in the reinforcement in conjunction with the square cube of yield strength indicates an enhancement in strength. In addition, if they are governing, flexural failure modes are highly dependent on the concrete strength. This is the case for specimen DB3, which has low concrete strength but, combined with the other structural parameters, showed high normalised strength (identified by the black square near the top of the graphs in Figure 12).

Flat slab members provided with transverse bars and with high reinforcement ratios ($\rho_l > 1{\cdot}0\%$) are generally governed by punching shear failure. The failure mode can differ depending on the layout and number of transverse bars. Although it

might not be the general case, members similar to those reported here (i.e. which are provided with well-anchored, equally spaced, double-headed shear studs arranged in a star-like shape and comply with the in-plane stud positioning requirements (i.e. distances from the column face)) fail in punching shear within the shear-reinforced region. Other in-plane layouts could lead to punching outside of the shear-reinforced zone (when the shear stress outside the shear-reinforced zone is higher than the concrete can sustain) or by reaching the maximum punching capacity (for heavily shear-reinforced specimens). On the other hand, regardless of the amount of transverse reinforcement, low flexural reinforcement could lead to flexural failure ratios (e.g. $\rho_l = 0{\cdot}5\%$).

Concluding remarks

This paper summarises the test programme and the analytical studies done on ten large-scale, square, interior flat slab specimens with and without transverse reinforcement connected to square stub columns. The experimental arrangement and specimen details, and the results and observations obtained from the tests are provided and discussed. Particular attention is given to the influence of a number of key parameters that characterise the behaviour at the ultimate state, such as slab thickness and the layout and amount of flexural and transverse reinforcement. The test results enabled direct assessment of the governing factors that affect the behaviour and failure mode of flat slab members at their connection to interior columns. Based on the experimental results, analyses and comparisons, the following conclusions can be drawn:

- Punching failure is potentially governing in flat slabs at interior columns, even if the slabs are shear reinforced.
- Flexural failure potentially governs at low flexural reinforcement ratios, whereas punching shear occurs at average to high flexural reinforcement ratios, and the failure mode is a function of the layout and the number of transverse bars.
- At low reinforcement ratios, the presence of transverse reinforcement has minimal influence on the ultimate strength.
- The use of double-headed shear studs was effective, leading to enhanced punching shear strength and deformability in the case of slabs in which flexural failure was not the governing mode.
- Design codes tend to give conservative estimates in the case of punching without shear reinforcement and punching within the shear-reinforced region for thick slabs ($h > 230$ mm), and increased accuracy for thin ones.
- Eurocode 2 tends to give effective results for the ultimate capacity of slabs at interior connections, accounting for the limit on yield strength of transverse reinforcement.
- ACI 318-14 gives conservative results, with the accuracy increasing with decreasing slab thickness.
- Model Code 2010 and the CSCT give good estimates of the ultimate punching shear strength. Better accuracy is obtained when a higher degree of refinement is used (LoA3 for Model Code 2010).

Acknowledgements

The support of JDA Jordahl Pfeiffer Romania, which provided the shear-reinforcing materials, Gama Construct SRL Sibiu, which contributed the steel reinforcement and moulds for the fabrication of the test specimens, and Hasel Industrial SRL Tg. Mureş, which provided instrumentation devices, is gratefully acknowledged.

REFERENCES

ACI (American Concrete Institute) (2014) ACI 318-14: Building code requirements for structural concrete and commentary. ACI, Farmington Hills, MI, USA.

Bazant ZP and Cao Z (1987) Size effect in punching shear failure of slabs. *ACI Structural Journal* **84(1)**: 44–53.

Beutel R and Hegger J (2002) The effect of anchorage on the effectiveness of the shear reinforcement in the punching zone. *Cement & Concrete Composites* **24(6)**: 539–549.

Birkle G and Digler WH (2008) Influence of slab thickness on punching shear strength. *ACI Structural Journal* **105(2)**: 180–188.

Bompa DV and Oneţ T (2015) Punching shear strength of RC flat slabs at interior connections to columns. *Magazine of Concrete Research* **68(1)**: 24–42, http://dx.doi.org/10.1680/macr.14.00402.

Carvalho AL, Melo SG, Gomes RB and Regan PE (2011) Punching shear in post-tensioned flat slabs with stud rail shear reinforcement. *ACI Structural Journal* **108(5)**: 523–531.

CEN (European Committee for Standardization) (2004) EN 1992-1-1, Eurocode 2: Design of concrete structures. Part 1-1: general rules for buildings. CEN, Brussels, Belgium.

Eligehausen R, Vocke H, Clauss A, Furche J and Bauermeister U (2003) Neue durchstanzbewehrung für elementdecken. *Beton- und Stahlbetonbau* **98(6)**: 334–344 (in German).

Elstner RC and Hognestad E (1956) Shearing strength of reinforced concrete slabs. *ACI Journal* **53(2)**: 29–58.

Fernandez Ruiz M and Muttoni A (2009) Applications of critical shear crack theory to punching of reinforced concrete slabs with transverse reinforcement. *ACI Structural Journal* **106 (4)**: 485–494.

fib (Federation Internationale du Beton) (2001) *Punching of Structural Concrete Slabs*. fib, Lausanne, Switzerland, fib bulletin 12.

fib (2012) *Model Code 2010*. fib, Lausanne, Switzerland, fib bulletins 65 and 66.

Gomes RB and Regan PE (1999a) Punching resistance of RC flat slabs with shear reinforcement. *Journal of Structural Engineering* **125(6)**: 684–693.

Gomes RB and Regan PE (1999b) Punching strength of slabs reinforced for shear with offcuts of rolled steel I-section beams. *Magazine of Concrete Research* **51(2)**: 121–129, http://dx.doi.org/10.1680/macr.1999.51.2.121.

Guandalini S, Burdet O and Muttoni A (2009) Punching tests of slabs with low reinforcement ratios. *ACI Structural Journal* **106(1)**: 87–95.

Hallgren M (1996) *Punching Shear Capacity of Reinforced High-Strength Slabs*. PhD thesis, KTH Stockholm, Stockholm, Sweden, TRIT-BKN, Bulletin 23.

Kinnunen S and Nylander H (1960) Punching of concrete slabs without shear reinforcement. *Transactions of the Royal Institute of Technology* **158(3)**: 1–112.

Lips S, Fernández Ruiz M and Muttoni A (2012) Experimental investigation on punching strength and deformation capacity of shear-reinforced slabs. *ACI Structural Journal* **109(6)**: 889–900.

Moe J (1961) *Shearing Strength of Reinforced Concrete Slabs and Footings under Concentrated Loads*. Portland Cement Association, Skokie, IL, USA, Bulletin D47.

Muttoni A (2008) Punching shear strength of reinforced concrete slabs without transverse reinforcement. *ACI Structural Journal* **105(4)**: 440–450.

Rizk E, Marzouk H and Hussein A (2011) Punching shear of thick plates with and without shear reinforcement. *ACI Structural Journal* **108(5)**: 581–591.

Tolf P (1992) *Effect of Slab Thickness on Punching Shear Strength*. Department of Structural Mechanics and Engineering, Royal Institute of Technology, Stockholm, Sweden.

WHAT DO YOU THINK?

To discuss this paper, please submit up to 500 words to the editor at journals@ice.org.uk. Your contribution will be forwarded to the author(s) for a reply and, if considered appropriate by the editorial panel, will be published as a discussion in a future issue of the journal.